Manju et al | Article 10971
J Pure Appl Microbiol. 2026;20(2):1571-1589. doi: 10.22207/JPAM.20.2.46
Received: 18 September 2025 | Accepted: 26 December 2025
Published Online: 04 June 2026

P-ISSN: 0973-7510; E-ISSN: 2581-690X

RESEARCH ARTICLE OPEN ACCESS

Computational Insights into Bioactive Metabolites from *Burkholderia stagnalis* as Potential Inhibitors of Glutathione S-Transferase (GST) in *Escherichia coli*

K. Manju[1], Ravikumara[1], Syed Baker[1], S. Satish[2], H. Shayista[3], H.K. Ranjini[4], M.P. Manasa[5], T.K. Pavan[1] and S. Niranjan Raj[1]*

[1]Department of Studies in Microbiology, Karnataka State Open University, Mysuru, Karnataka, India.
[2]Department of Microbiology, University of Mysuru, Mysuru, Karnataka, India.
[3]Department of Biotechnology, JSS Science and Technology University, Mysuru, Karnataka, India.
[4]Department of Microbiology, School of Life Science, JSS Academy of Higher Education and Research, Mysuru, Karnataka, India.
[5]Department of Chemistry, Yuvaraja's College, University of Mysuru, Karnataka, India.

Abstract

Bioactive metabolites produced by the *Burkholderia* genus, especially within the *Burkholderia pseudomallei-thailandensis-mallei* (Bptm) group, are vital for survival in diverse environments, influencing ecological interactions and contributing to the adaptability of these bacteria. This study focused on the screening of bacteria for antibacterial activity, further culturing in broth. The cell free extract was treated with the equal amount of ethyl acetate where after Vortex the organic phase was vacuum dried and subjected to for the functional group analysis via FTIR Where it revealed the presence of peak at 3352 cm^{-1}, 2177 cm^{-1} and 1637 cm^{-1} corresponding to amine, nitrile alkene group respectively. GC-MS analysis presence of 24 bioactive compounds, followed by the ADME and toxicity test were done to narrow down the metabolites. Finally, the docking study was done against Glutathione S-Transferase. Glutathione S-transferase (GST) as the target enzyme because GSTs are key detoxification proteins that conjugate glutathione to xenobiotics and reactive intermediates, thereby protecting bacteria from oxidative damage and chemical stress. In *E. coli*, GST activity has been implicated in tolerance to multiple antibiotics and other toxic compounds by detoxifying or neutralising them, which can indirectly contribute to antimicrobial resistance. Targeting GST therefore provides a mechanistically relevant way to evaluate whether microbes-derived metabolites can interfere with this detoxification system and potentially sensitise bacteria to existing antibiotics. Four bioactive compounds were docked against GST and Cyclobutyl tridecyl phthalate exhibited the highest score of -8.9 kcal/mol followed by Phthalic acid, 4-cyanophenyl nonyl ester -7 kcal/mol, 1,3-Dioxolane, 4-ethyl-5-octyl-2,2-bis(trifluoromethyl)-, trans- with -6.9 kcal/mol, Pentalamide with a score of -6.3 kcal/mol and Meta-chlorambucil was used as control. The in-vivo evaluation can be performed to evaluate the present study.

Keywords: Metabolites, Ligands, Molecular Docking, Antimicrobial Resistance, *Burkholderia* spp.

***Correspondence:** niruraj@gmail.com

Citation: Manju K, Ravikumara, Baker S, et al. Computational Insights into Bioactive Metabolites from *Burkholderia stagnalis* as Potential Inhibitors of Glutathione S-Transferase (GST) in *Escherichia coli*. *J Pure Appl Microbiol.* 2026;20(2):1571-1589. doi: 10.22207/JPAM.20.2.46

INTRODUCTION

Microbial bioactive metabolites represent a rich source of novel metabolites for the drug discovery and development. Among the microbial diversity, bacteria act as repertoire of diverse class of metabolites.[1] In recent times advancement in molecular biology which has provided sophisticated tools to explore microbial biosynthesis and study metabolomics of bacteria. These bacteria upon isolation and screening can secret metabolites bearing activity. Soil microbes secrete various bioactive metabolites that facilitate ecological interactions and have biotechnological applications.[2] *Burkholderia*, a versatile genus classified within the phylum Proteobacteria, encompasses a diverse range of species isolated from various environments, including soil, plant roots, and clinical settings.[3] Initially identified in 1992, the genus has expanded significantly and now includes both pathogenic strains and beneficial species that promote plant growth. The two major groups within *Burkholderia* are the *Burkholderia cepacia* complex (BCC) and the *Burkholderia pseudomallei* complex (BPC), with ongoing reclassifications leading to the emergence of genera such as *Paraburkholderia* and *Caballeronia*. Recent studies on *Burkholderia* have emphasized genome-based classification, genomic diversity analysis, and pan-genome analysis, revealing the complexities of this genus. The taxonomic position of Taxon K within the BCC has been reevaluated, highlighting the significance of genomic data in classification efforts.[4,5] Previous study identified various antimicrobial bioactive metabolites produced by *Burkholderia*, linking these metabolites to their taxonomy. Notable findings include the discovery of new antimicrobial bioactive metabolites and the identification of compounds like Bactobolin in *Burkholderia thailandensis*. Additionally, siderophores associated with plant growth promotion have been found in pathogenic strains, highlighting the ecological roles of these metabolites, revealing their capacity to produce a wide array of bioactive metabolites with applications in agriculture, biocontrol, and medicine.[6]

In recent years, antibiotic resistance (ABR) has emerged as a critical global health crisis. Projections indicate that by 2050, ABR could lead to as many as 10 million deaths worldwide, while by 2030, it may push 24 million people into extreme poverty.[7] The most vulnerable populations include infants, adults, and the elderly. A clinical report on resistant bacteria highlighted alarming resistance rates across all six World Health Organization (WHO) regions. In five of these regions, *E. coli* exhibited over 50% resistance to fluoroquinolones and third-generation cephalosporins. Similarly, *Klebsiella pneumoniae* showed more than 50% resistance to third-generation cephalosporins in all six WHO regions.[8,9] Glutathione S-transferases (GSTs; EC 2.5.1.18) are cytosolic dimeric enzymes that catalyse the conjugation of reduced glutathione (GSH) to electrophilic xenobiotics and endogenous toxic intermediates, thereby increasing their solubility and facilitating subsequent efflux or metabolism. In bacteria, GSTs are widely distributed and have been grouped into several classes; they play key roles in the biodegradation of xenobiotics, protection against oxidative and chemical stress, and in some cases antimicrobial drug resistance by detoxifying antibiotic-derived reactive species. The canonical GST from *Escherichia coli* is a cytosolic β-class enzyme whose three-dimensional structure has been solved at 2.1Å resolution in complex with a glutathione analogue (PDB ID: 1A0F). EGST forms a globular homodimer, with each 201-residue subunit composed of an N-terminal thioredoxin-like domain and a C-terminal all-α-helical domain; the active site consists of a conserved G-site that binds GSH and a hydrophobic H-site that accommodates electrophilic substrates. Structural and mutational analyses have identified Cys10 and His106 as key catalytic residues that help activate the thiol group of GSH and stabilise the transition state, underscoring the mechanistic importance of this enzyme in *E. coli* redox homeostasis. Consistent with this central role, bacterial GSTs are up-regulated under oxidative or xenobiotic stress and can contribute to tolerance against multiple toxic compounds, including antibiotics, by detoxifying reactive intermediates before they damage essential macromolecules.[10,11]

In silico methods, essential for modern drug discovery, predict and analyze molecular behavior, particularly of metabolites. Molecular docking evaluates ligand-receptor binding affinities and spatial orientation.[12] ADME analysis

provides insights into pharmacokinetic properties, crucial in medicinal chemistry. Drug-likeness assessments offer rapid, cost-effective evaluations of pharmacokinetic characteristics.[13] These techniques narrow the drug discovery process and improve understanding of drug candidate interactions with biological systems, aiding the development of effective therapeutics. Integrating these methodologies streamlines exploration and identifies promising drug candidates with favorable pharmacological profiles.[14] In the present study where screening and isolation of the rhizospheric bacteria *Burkholderia stagnalis* for their antibacterial property. Further partial purification and *in silico* evaluation of the potent bioactive metabolites derived from *Burkholderia stagnalis* against Glutathione S-Transferase from *E. coli.* This integrated strategy stands as the base for the further evaluation.

MATERIALS AND METHODS

Isolation, Screening and extraction of bioactive metabolites

1 g of Rhizospheric soil from Western Ghat Chikkamagaluru, Karnataka, India, was subjected to serial dilution. The dilution in the range of 10^{-4}, 10^{-5}, 10^{-6} dilution were spread on nutrient agar, followed by incubation until the colonies are observed at 37 °C.[15] Different isolates were screened for antimicrobial activity via agar overlay assay. The isolates displaying significant activity was further selected for large scale cultivation.[16] The broth culture was extracted twice

a b

Figure 1. Spread plate result (a) and broth culture growth (b)

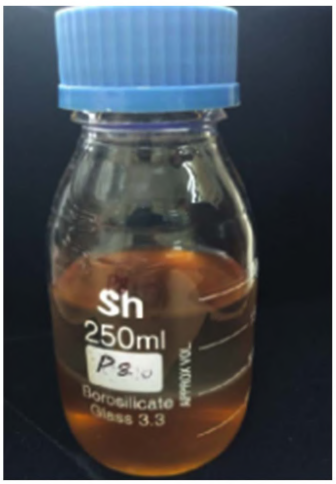

Figure 2. Two layer separation of ethyl acetate and broth for secondary metabolite extraction

using ethyl acetate as a solvent in a ratio of 1:1 and was vortexed for 20 minutes. The organic phase was further concentrated by evaporation followed by drying at 40 °C.[17]

Biophysical characterization of bioactive metabolites

The crude extract was analyzed using a Perkin Elmer spectrophotometer to obtain the Fourier Transform Infrared (FTIR) spectrum.[18] Gas Chromatography-Mass Spectrometry (GC-MS) was performed within the desired parameters, helium as carrier gas performed at temperature 250 °C under ionized mod. The results spectra were matched with NIST library.[19]

Table 1. Functional group of the crude extract of *Burkholderia stagnalis*

Peak (cm^{-1})	Functional Group	Bond	Description
3352	Amine	N-H stretch	Broad peak, indicative of N-H stretching in primary or secondary amines.
2177	Nitrile	Ca=C stretch	Sharp peak, indicates the presence of a nitrile group.
2149	Alkyne	Ca=C stretch	Indicates the presence of a terminal alkyne group.
2035	Alkene	C=C stretch	May indicate a cumulated double bond system (allene).
1637	Aromatic/Alkene	C=C stretch	Indicates the presence of aromatic compounds or alkenes.
627	Alkyl halide	C-Cl stretch	Indicates the presence of an alkyl chloride.

Table 2. Bioactive compounds of the crude extract of *Burkholderia stagnalis*

RT	Name	Formula	MW
3.2	Octane	$C_{10}H_{22}$	142.28
3.2	Butanol,	$C_8H_{16}O_2$	144.21
3.2	Pentaerythritol	$C_5H_{12}O_4$	136.15
3.2	Ethyl Acetate	$C_4H_8O_2$	88.11
12.7	Hexane	C_8H_{18}	114.23
17	Cyclobutyl tridecyl phthalate	$C_{25}H_{38}O_4$	402.57
17	Phthalic acid, 4-cyanophenyl nonyl ester	$C_{24}H_{27}NO_4$	393.48
17	Tylophorine	$C_{26}H_{40}O_4$	416.59
17.5	Capric Acid	$C_{10}H_{20}O_2$	172.26
17.5	Undecane	$C_{11}H_{24}$	156.31
17.5	Heptane, 2,4-dimethyl-	C_9H_{20}	128.26
18.8	1-Hexadecyne	$C_{16}H_{30}$	222.41
18.8	Heptadecadiene	$C_{17}H_{32}$	236.44
18.8	Pentalamide	$C_{12}H_{17}NO_2$	207.27
18.8	octadecyne	$C_{18}H_{34}$	250.46
18.8	1,3-Dioxolane, 4-ethyl-5-octyl-2,2-bis(trifluoromethyl)-, trans-	$C_{15}H_{24}F_6O_2$	350.34
18.8	Nonadecyl 2,4,5-trifluoro-3-methoxybenzoate	$C_{27}H_{43}F_3O_3$	472.62
18.8	Octacosadiene	$C_{28}H_{54}$	390.73
18.8	Ethyl acetoacetate	$C_6H_{10}O_3$	130.14
19.7	2,4,6-Cycloheptatrien-1-one, 3,5-bis-trimethylsilyl-	$C_{13}H_{22}OSi_2$	250.48
19.7	Hexamethylcyclotrisiloxane	$C_6H_{18}O_3Si_3$	222.46
19.7	Phenol, 2,4-bis-(1,1-dimethylethyl), TMS	$C_{17}H_{30}OSi$	278.51
19.7	4-(4-Hydroxyphenyl)-4-methyl-2-pentanone	$C_{15}H_{24}O_2Si$	264.44
19.7	Tris(tert-butyldimethylsilyloxy)arsane	$C_{18}H_{45}AsO_3Si_3$	510

Molecular characterization of isolate

The isolate showing significant activity underwent molecular characterization using universal primers. Amplification was performed, and the resulting product was purified for sequencing. BLAST search at NCBI was utilized to identify the closest related organism, and phylogenetic was constructed.[20]

Computational analysis

Preparation of ligand

For the docking study, the 3D structure and canonical SMILES were retrieved from online database PubChem, and further the minimization of charge was done by Open Babel version and then metabolites were converted into Protein data bank format.[21]

ADME and toxicity test

The tests were performed in Swiss ADME, toxicity test was performed in ProTox-3.0 server. Further GUSAR software was utilized to estimate LD_{50} values in rats via oral, intravenous, intraperitoneal, and subcutaneous routes.[22]

Target protein preparation

GST from *E. coli* is a crucial enzyme involved in detoxifying harmful compounds through the conjugation of glutathione (GSH). The enzyme is a homodimer composed of two identical subunits, each consisting of 201 amino acids. Its structure features an N-terminal domain and a C-terminal domain, with the active site located between them. This enzyme catalyzes the addition of GSH to xenobiotic substrates, facilitating their excretion Among 24 bioactive metabolites Tris (tert-butyldimethylsilyloxy)arsane from the cell and thereby protecting against oxidative stress and chemical toxicity. In the context of antibiotic resistance, GST's can contribute to the development of antimicrobial resistance by detoxifying various antibiotics, rendering them ineffective. The crystal structure of GST (PDB ID: 1A0F, resolution: 2.10Å) was drawn from RCSB, processed to remove water and small ligands, and prepared using Bio Nova Discovery Studio 2024 to incorporate polar hydrogens and combine non-polar hydrogens for energy minimization and geometry optimization. Kollman charges were assigned, and the receptor structure was saved in PDBQ format before docking.[23]

Molecular docking and MD simulation

Molecular docking was carried out using AutoDock Vina, integrated within PyRx 0.8,

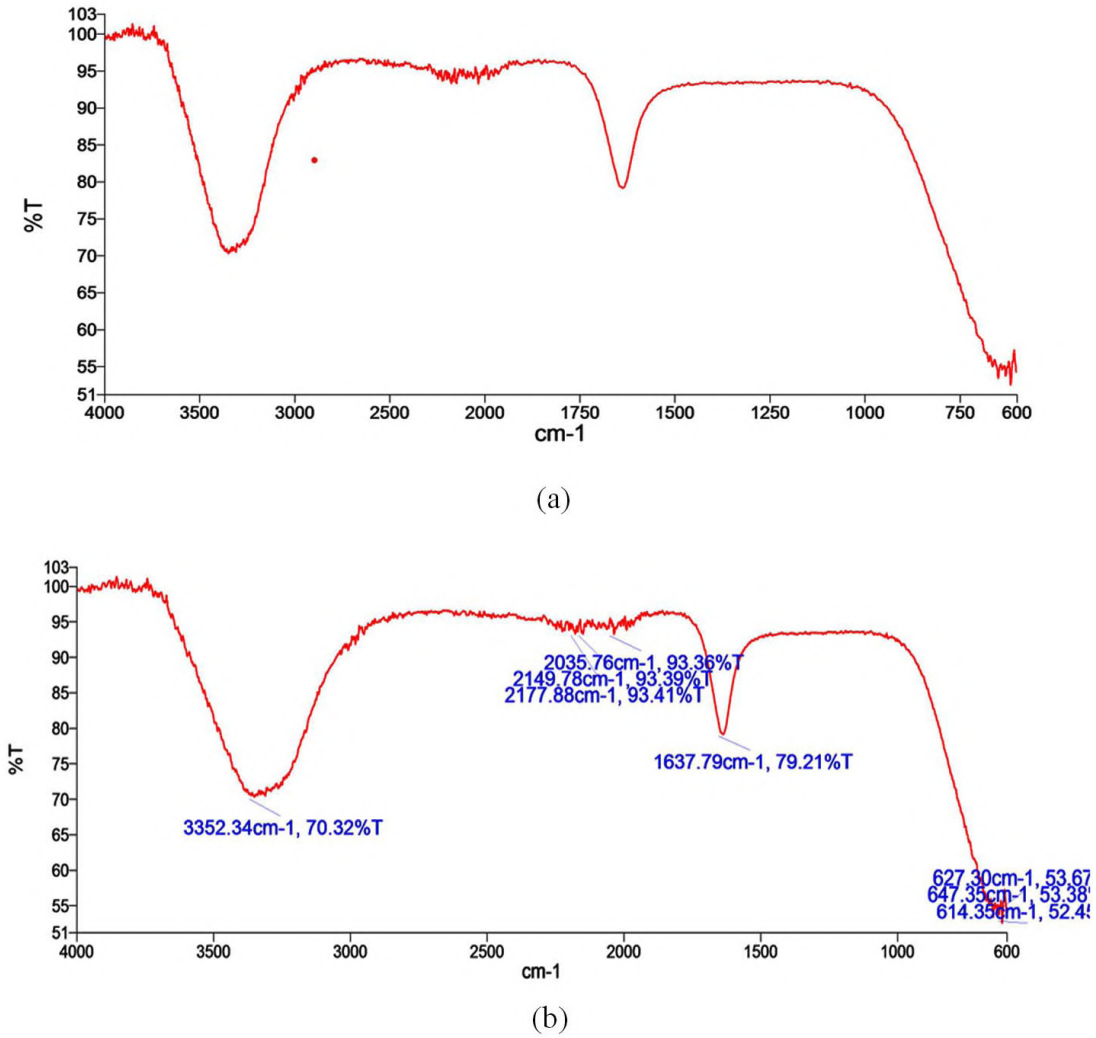

Figure 3. Showing FTIR peak (a) corresponding to various peak range (b)

employing the Lamarckian Genetic Algorithm to analyze ligand interactions with the active site of GST. The gride box set for X: 57.3699, Y: -33.0833 and Z: 58.2943. The docking parameters were set to default, with protein coordinates saved in PDBQT format. Binding affinities, measured in kilocalories per mole (kcal/mol), were used to determine the optimal docking pose, identified as the conformation with the lowest binding energy. Post-docking, the best ligand binding poses were visualized, and their interactions with the GST protein were analyzed using BIOVIA Discovery Studio Visualizer. Molecular dynamic simulations were performed using the IMODS server.[24-26]

RESULTS

Isolation, Screening and extraction of bioactive metabolites

After the serial dilution the sample were plated on the plate, among the different isolates obtained through agar overlay assay which indicate the antibacterial property of the isolate (Figure 1). The culture broth was centrifuged, after which the cell free extract was subjected for extraction of crude metabolites. The organic phase (Figure 2) upon drying gave crude extract which was dissolved in 100 µL ethyl acetate.

Biophysical characterization of bioactive metabolites

FTIR analysis of crude revealed prominent peaks at 3352 cm^{-1}, 2035 cm^{-1}, 2149 cm^{-1}, 2177 cm^{-1}, 1637 cm^{-1}, and 627 cm^{-1} (Figure 3). Table 1 details the potential functional group assignments corresponding to these peaks. Significant shifts were observed at 3352 cm^{-1} and 1637 cm^{-1} in the bacterial culture extract spectra, indicating notable chemical modifications. GC-MS analysis revealed 24 bioactive metabolites out of which Cyclohexanecarboxamide, Nonadecyl ester, 4-tert-Octylphenol, Pentaerythritol, cyclobutyl tetradecyl ester, Heptane were few of major compounds (Figure 4 and Table 2).

Molecular profiling

Molecular profiling, combined with sequence alignment using the NCBI BLAST database, revealed that the bacterium exhibited similarity to *Burkholderia stagnalis*. After which the sequence was deposited in GenBank and allocated the accession number PV151462. The phylogenetic tree further showed the taxonomic relationship between identified bacteria and *Burkholderia stagnalis* (Figure 5a). The circular genome map of *Burkholderia stagnalis* visually illustrates elevated GC content and a uniform

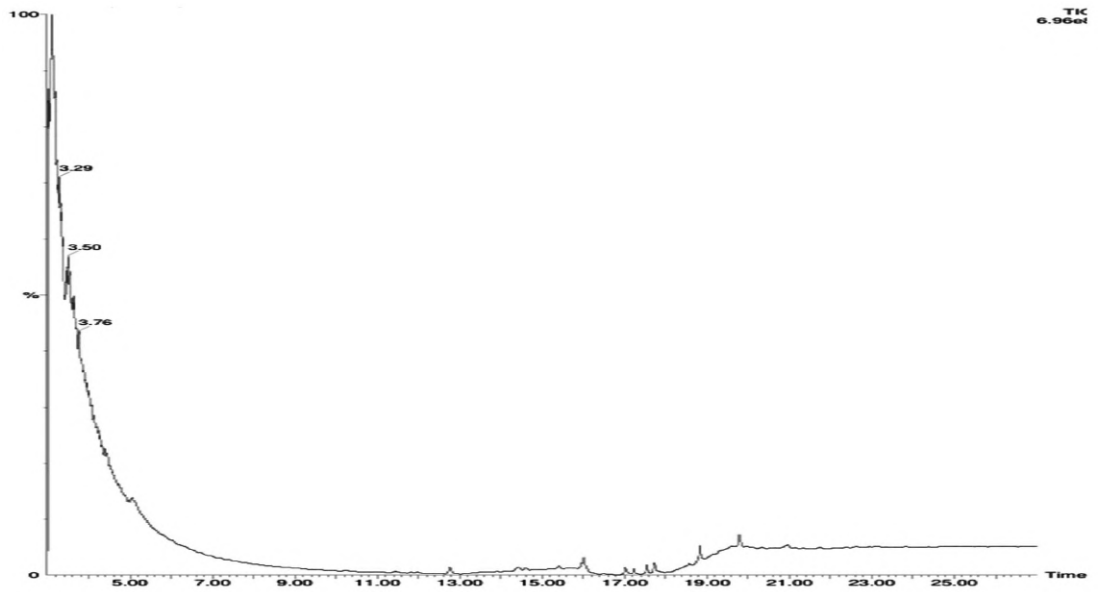

Figure 4. GC-MS chromatogram of the crude extract from *Burkholderia stagnalis*

Table 3. ADME validation of the metabolites from *Burkholderia stagnalis*

Name	Formula	MW	Heavy atoms	Aromatic heavy atoms	Rotatable bonds	H-bond acceptors	H-bond donors	TPSA	iLOGP	GI absorption	Lipinski violations	Synthetic Accessibility
Octane	$C_{10}H_{22}$	142.28	10	0	7	0	0	0	3.29	Low	1	1.62
Butanol	$C_8H_{16}O_2$	144.21	10	0	6	2	1	37.3	1.95	High	0	1.47
Pentaerythritol	$C_5H_{12}O_4$	136.15	9	0	4	4	4	80.92	0.82	High	0	1.12
Ethyl Acetate	$C_4H_8O_2$	88.11	6	0	1	2	1	37.3	1.11	High	0	1
Hexane	C_8H_{18}	114.23	8	0	5	0	0	0	2.88	Low	1	1.42
Cyclobutyl tridecyl phthalate	C_8H_{18}	402.57	29	0	2	4	3	77.76	3.29	High	0	6.17
Phthalic acid, 4-cyanophenyl nonyl ester	$C_{24}H_{27}NO_4$	393.48	29	14	4	5	0	40.16	4	High	0	3.48
Tylophorine	$C_{26}H_{40}O_4$	416.59	30	0	6	4	0	52.6	4.64	High	1	5.58
Capric Acid	$C_{10}H_{20}O_2$	172.26	12	0	8	2	1	37.3	2.5	High	0	1.67
Undecane	$C_{11}H_{24}$	156.31	11	0	8	0	0	0	3.59	Low	1	1.72
Heptane, 2,4-dimethyl-	C_9H_{20}	128.26	9	0	6	0	0	0	3.06	Low	1	1.52
1-Hexadecyne	$C_{16}H_{30}$	222.41	16	0	12	0	0	0	4.56	Low	1	4.14
Heptadecadiene	$C_{17}H_{32}$	236.44	17	0	13	0	0	0	4.67	Low	1	4.25
Pentalamide	$C_{12}H_{17}NO_2$	207.27	15	6	4	2	1	38.33	2.78	High	0	1.95
octadecyne	$C_{18}H_{34}$	250.46	18	0	4	0	0	0	3.96	Low	1	3.07
1,3-Dioxolane, 4-ethyl-5-octyl-2,2-bis (trifluoromethyl)-, trans-	$C_{15}H_{24}F_6O_2$	350.34	23	0	3	8	2	40.46	2.68	Low	0	4.14
Nonadecyl 2,4,5-trifluoro-3-methoxybenzoate	$C_{27}H_{43}F_3O_3$	472.62	33	6	21	6	0	35.53	6.45	Low	1	4.12
Octacosadiene	$C_{28}H_{54}$	390.73	28	0	16	0	0	0	6.54	Low	1	3.81
Ethyl acetoacetate	$C_6H_{10}O_3$	130.14	9	0	3	3	1	54.37	1.06	High	0	1.04
2,4,6-Cycloheptatrien-1-one, 3,5-bis-trimethylsilyl-	$C_{13}H_{22}OSi_2$	250.48	16	6	1	1	1	20.23	3.31	High	0	3.8
Hexamethylcyclo-trisiloxane	$C_6H_{18}O_3Si_3$	222.46	12	0	0	3	0	27.69	3.39	High	0	4.34
Phenol, 2,4-bis-(1,1-dimethylethyl), TMS	$C_{17}H_{30}OSi$	278.51	19	6	5	1	0	9.23	4.14	Low	1	3.03
4-(4-Hydroxyphenyl)-4-methyl-2-pentanone	$C_{15}H_{24}O_2Si$	264.44	18	0	12	2	0	26.3	3.81	High	0	3.63
Tris (tert-butyldimethyl-silyloxy) arsane	$C_{18}H_{45}AsO_3Si_3$	510	25	0	9	3	0	27.69	0	Low	0	5.7

Table 4. Toxicity assessment of the selected compound.

Compound	Formula	hepa-toxicity	carcino-toxicity	immuno-genicity	muta-toxicity	cyto-genicity	AhR	AR	PPAR-Gamma	HSE	p53	LD_{50} mg/kg	toxicity class
Pentalamide	$C_{12}H_{17}NO_2$	IA	IA	IA	IA	IA	IA	IA	IA	IA	IA	16	2
1,3-Dioxolane, 4-ethyl-5-octyl-2,2-bis (trifluoromethyl)-, trans-	$C_{15}H_{24}F6O_2$	IA	IA	IA	IA	IA	IA	IA	IA	IA	IA	1750	4
Cyclobutyl tridecyl phthalate	$C_{25}H_{38}O_4$	IA	IA	IA	IA	IA	IA	IA	IA	IA	IA	50	2
Phthalic acid, 4-cyanophenyl nonyl ester	$C_{24}H_{27}NO_4$	IA	A	A	IA	A	IA	IA	IA	IA	IA	100	3

Table 5. Evaluation of Lethal Dose (LD 50) Values in Murine Models via Multiple Delivery Methods

Compound	Rat IP LD_{50} Log_{10} (mmol/kg)	Rat IV LD_{50} log_{10} (mmol/kg)	Rat Oral LD_{50} log_{10} (mmol/kg)	Rat SC LD_{50} log_{10} (mmol/kg)	Rat IP LD_{50} (mg/kg)	Rat IV LD_{50} (mg/kg)	Rat Oral LD_{50} (mg/kg)	Rat SC LD_{50} (mg/kg)	Rat IP LD_{50} Classi-fication	Rat IV LD_{50} Classi-fication	Rat Oral LD_{50} Classi-fication	Rat SC LD_{50} Classi-fication
Pentalamide	0,473 in AD	-0,384 in AD	0,993 in AD	0,208 in AD	1041,000 in AD	144,800 in AD	3448,000 in AD	565,400 in AD	Class 5 in AD	Class 4 in AD	Class 5 in AD	Class 4 in AD
Cyclobutyl tridecyl phthalate	-0,070 in AD	-1,362 in AD	0,504 in AD	-0,400 in AD	342,900 in AD	17,480 in AD	1285,000 in AD	160,400 in AD	Class 4 in AD	Class 3 in AD	Class 4 in AD	Class 4 in AD
Phthalic acid, 4-cyanophenyl nonyl ester	-0,310 in AD	-1,088 in AD	-0,145 out of AD	-0,014 in AD	192,900 in AD	32,110 in AD	281,600 out of AD	381,100 in AD	Class 4 in AD	Class 3 in AD	Class 3 in AD	Class 4 in AD
1,3-Dioxolane, 4-ethyl-5-octyl-2, 2-bis (trifluoro-methyl)-, trans-	-0,208 in AD	-1,042 in AD	0,103 in AD	0,345 in AD	128,300 in AD	18,810 in AD	262,800 in AD	458,800 in AD	Class 4 in AD	Class 3 in AD	Class 3 in AD	Class 4 in AD

distribution of open reading frames (ORFs) (Figure 5b).

Computational analysis

The drug-likeness of 24 metabolites derived from *Burkholderia stagnalis* (Table 3). Using the SwissADME server. Out of these, 24 metabolites exhibited a logP value within the acceptable range of 0-5 rest 2 compound Nonadecyl ester 1,1'-(2-tridecyl-1,3-propanediyl) bis- were out of range more than 5. All bioactive metabolites have a acceptable range for for hydrogen bond acceptors (≤10), H bond donors (≤5), the TPSA with less than 140 $Å^2$. Among 24 bioactive metabolites Tris(tert-butyldimethylsilyloxy) arsane had a molecular weight of 510 and 9 compounds fell below 200 Octane, Butanol, Pentaerythritol, Ethyl Acetate, Pentanoic acid, 3-methyl-4-oxo-, Hexane, Pentanoic acid, 1,1-dimethylpropyl ester Octane, Heptane, 2,4-dimethyl. All the selected bioactive metabolites accepted the Lipinski's rule of 5 without violation which suggested the possibility of oral administration.

Selected bioactive metabolites obeyed 'Lipinski's rule of 5' without any violation suggesting their possibility of oral administration, The boiled egg plot evaluate the pharmacokinetic properties of the 24 bioactive metabolites, helping to predict their bioavailability and potential therapeutic applications (Figure 6). Only 4 compounds were further selected for the further toxicity test and docking study. The in silico toxicity test revealed Pentalamide and Cyclobutyl tridecyl phthalate fell under class 2, Phthalic acid, 4-cyanophenyl nonyl ester under class 3 and 1,3-Dioxolane, 4-ethyl-5-octyl-2,2-bis(trifluoromethyl)-, trans- was seen to be class 4 (Table 4). The LD_{50} values of these metabolites ranged from 16-1750 mg/kg, indicating potential toxicity concerns for oral deliver. GUSAR software was used to estimate the acute toxicity of selected compound, which provided LD_{50} values for different administration routes (intraperitoneal, intravenous, oral, and subcutaneous) in rats. The results indicate that 1,3-Dioxolane, 4-ethyl-5-octyl-2,2-bis(trifluoromethyl)-, trans- exhibited the lowest toxicity, classified as Class 5 in oral administration, suggesting it is relatively non-toxic. Cyclobutyl tridecyl phthalate and Phthalic acid, 4-cyanophenyl nonyl ester demonstrated moderate toxicity, with classifications ranging between Class 3 and Class 4, depending on the route of administration. Pentalamide was found to be slightly toxic in oral and subcutaneous routes (Class 4) but showed moderate toxicity via intravenous administration (Class 3). Notably, the oral LD_{50} values were generally higher, indicating lower toxicity compared to other administration routes. These findings highlight the significance of the route of exposure in determining the toxic effects of the compounds, with intravenous and intraperitoneal routes often exhibiting greater toxicity than oral and subcutaneous administrations (Table 5). The binding pocket of the protein is shown in the (Figure 7 and Table 6). The topology of the GST protein and 3D structure is shown in the Figure 8.

Table 6. Predicted Binding Pockets and Their Properties

Rank	Score	Probality	# of Residues	Avg Conservation
1	17.72	0.805	23	1.058
2	17.28	0.797	23	1.185
3	2.88	0.092	19	0.479
4	2.21	0.053	7	1.263

Molecular docking study

The metabolites, Pentalamide, 1,3-Dioxolane, 4-ethyl-5-octyl-2,2-

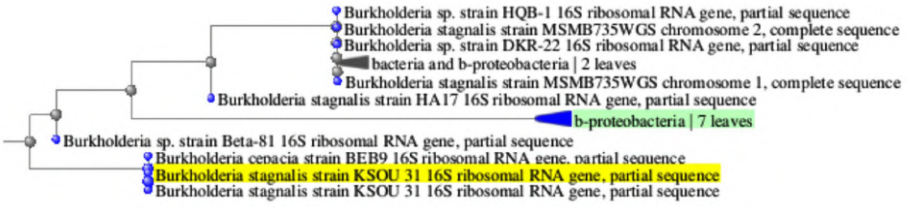

(a)

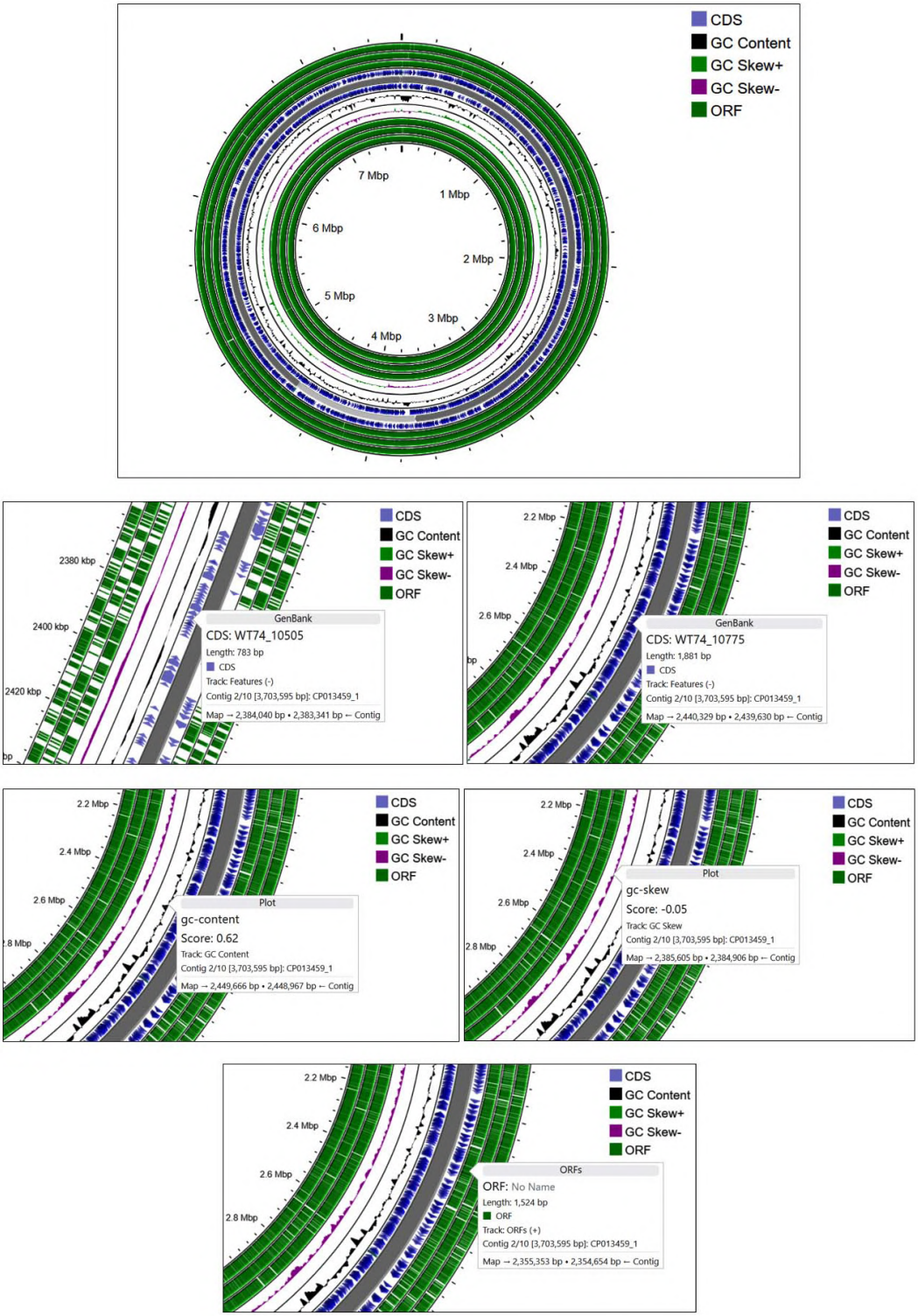

(b)

Figure 5. Phylogenetic tree showing the evolutionary relationship of the isolate (a) and its GC content analysis (b)

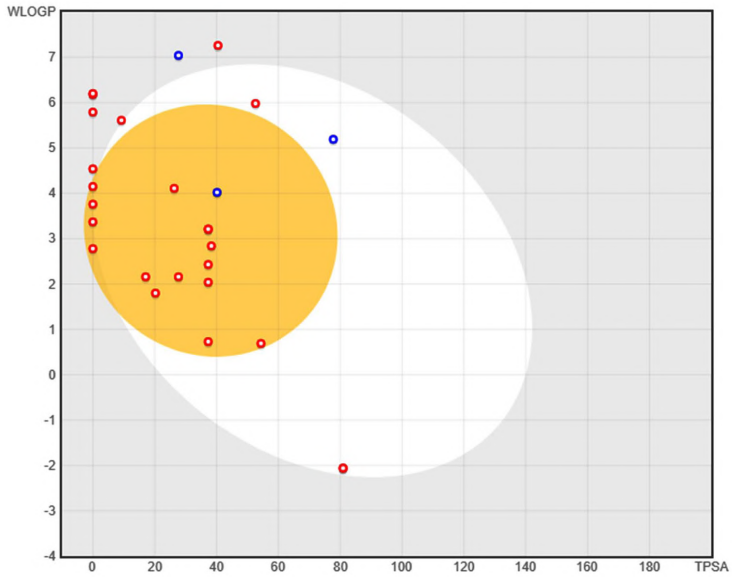

Figure 6. BOILED-Egg plot illustrating the absorption and blood-brain barrier permeability of 24 secondary metabolites. The x-axis represents topological polar surface area (TPSA), while the y-axis denotes lipophilicity (WLOGP). The yellow region (yolk) represents compounds predicted to be blood-brain barrier (BBB) permeable, while the white region (egg white) indicates compounds expected to be gastrointestinal (GI) tract permeable. Red circles denote non-P-glycoprotein substrates, while blue circles indicate P-glycoprotein substrates, which may be actively effluxed

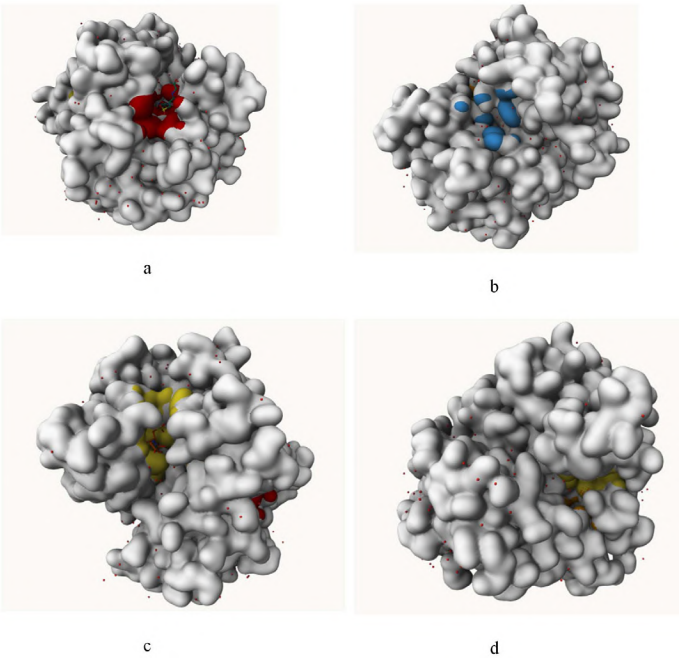

Figure 7. Visualization of predicted binding pockets in the protein structure showing different potential ligand-binding sites: (a) primary binding pocket highlighted in red, (b) secondary surface pockets highlighted in blue, (c) ligand-interacting cavity highlighted in yellow with bound conformation, and (d) another potential internal binding pocket highlighted in yellow within the protein structure

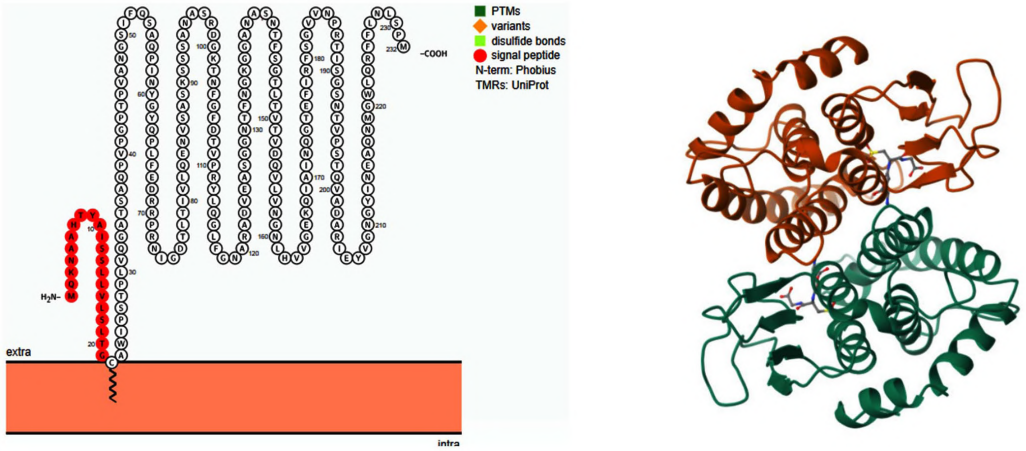

Figure 8. Transmembrane topology of Glutathione S-transferase (GST) from *E. coli* visualized using Protter v1.0. The image depicts the secondary structure of GST, highlighting key structural features. The signal peptide (red-orange) at the N-terminal region indicates the sequence responsible for targeting the protein to specific cellular locations. The protein spans the membrane multiple times, suggesting a possible role in detoxification processes. Post-translational modifications (PTMs), sequence variants, and disulfide bonds are annotated based on UniProt database predictions. This structural insight provides a basis for understanding GST's role in antimicrobial resistance (AMR) and its potential as a therapeutic target

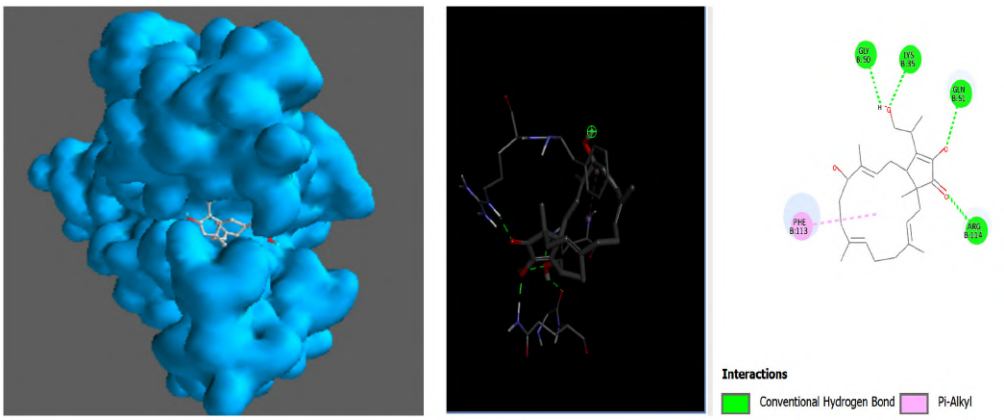

a

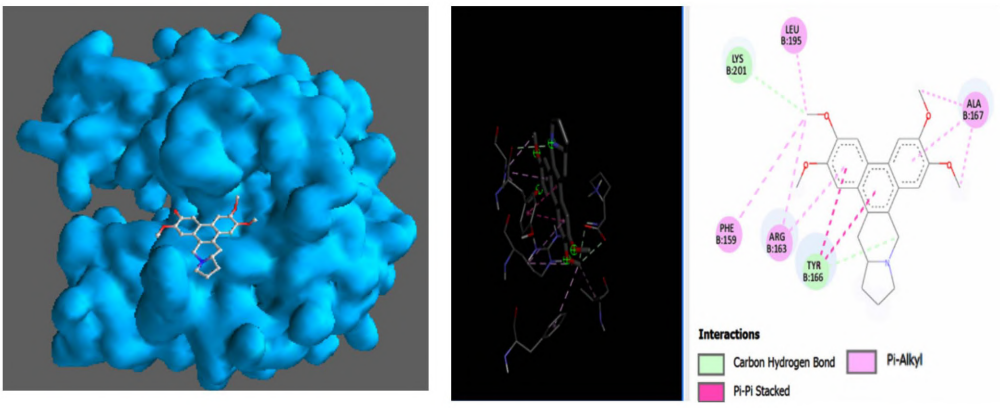

b

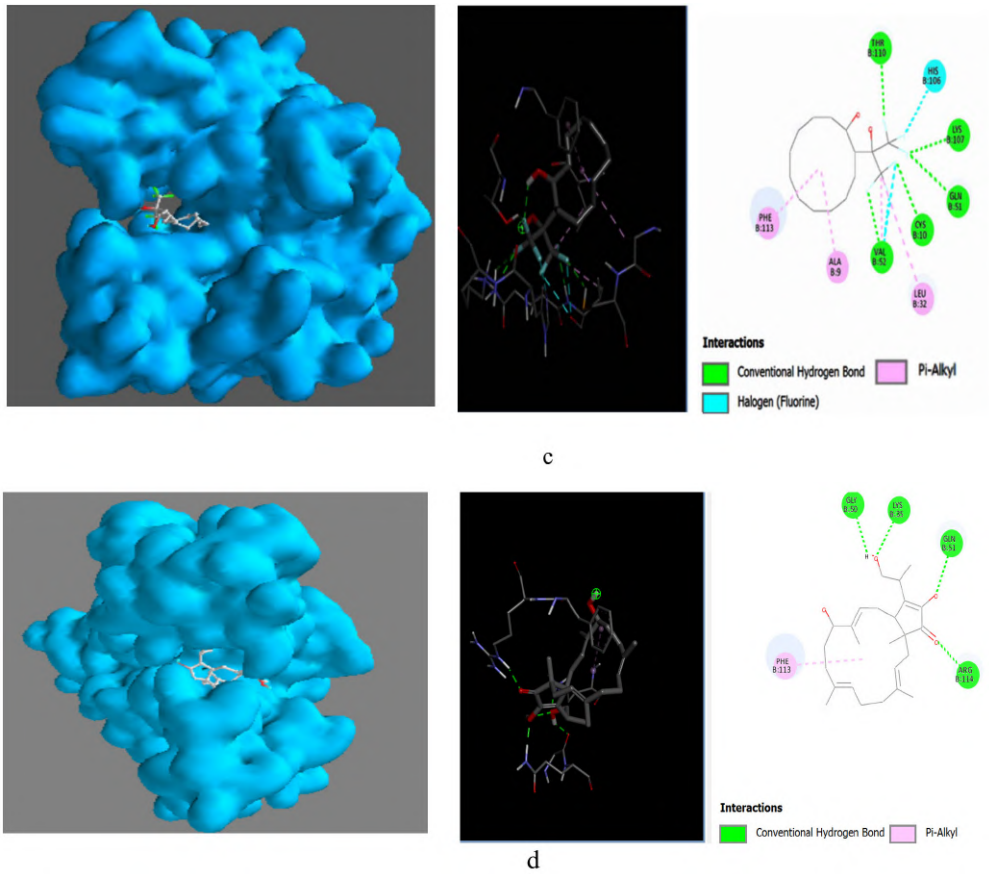

Figure 9. Molecular visualization of protein-ligand interactions was performed using Discovery Studio software. (a) GST with Cyclobutyl tridecyl phthalate, (b) GST with Phthalic acid, 4-cyanophenyl nonyl ester, (c) GST with 1,3-Dioxolane, 4-ethyl-5-octyl-2,2-bis(trifluoromethyl)-, trans-, (d) GST with Pentalamide

bis(trifluoromethyl)-, trans-, Cyclobutyl tridecyl phthalate, Phthalic acid, 4-cyanophenyl nonyl ester were docked against Glutathione S-Transferase (Table 7). The result showed Cyclobutyl tridecyl phthalate had a score of -8.7 followed by Phthalic acid, 4-cyanophenyl nonyl ester -7, then by 1,3-Dioxolane, 4-ethyl-5-octyl-2,2-bis(trifluoromethyl)-, trans- with -6.9 lastly Pentalamide with a score of -6.3, Meta-chlorambucil was used as control which had a score of -5.6. Cyclobutyl tridecyl phthalate forms conventional hydrogen bonds with Gly50, Lys35, and Gln51, significantly stabilizing it within the active site via enhanced molecular affinity. Alkyl interaction with Phe113 further stabilizes the ligand through hydrophobic forces and interaction with Arg114 maintains ligand orientation (Figure 9).

MD simulation

The iMODS simulation of the docked complex provided valuable insights into its dynamic properties. Key parameters such as deformability, variance, and eigenvalues were analysed, along with covariance maps and elastic networks, to assess the flexibility of the complex. Additionally, B-factors were examined to shed light on atomic mobility within the structure, offering a comprehensive understanding of its stability and dynamic behaviour, as illustrated in Figure 10. Validation of target protein-ligand complex structures Autodock 4.0 methodology

Table 7. Molecular docking score

Compound	Formula	MW	Structure	score
Cyclobutyl tridecyl phthalate	$C_{25}H_{38}O_4$	402.57	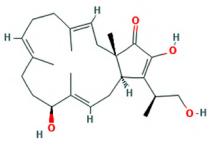	-8.9 g/mol
Phthalic acid, 4-cyanophenyl nonyl ester	$C_{24}H_{27}NO_4$	393.48	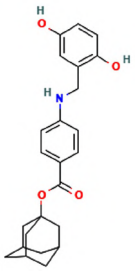	-7 g/mol
1,3-Dioxolane, 4-ethyl-5-octyl-2, 2-bis(trifluoromethyl)-, trans-	$C_{15}H_{24}F_6O_2$	350.34	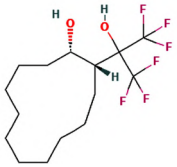	-6.9 g/mol
Pentalamide	$C_{12}H_{17}NO_2$	207.27	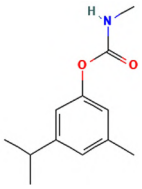	-6.3 g/mol
Meta-chlorambucil	$C_{14}H_{19}Cl_2NO_2$	304.2	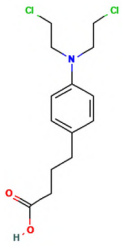	-5.6 g/mol

was validated with the respective co-crystallized ligands of target proteins to ensure the virtual screening process. Autodock 4.0 represents valid RMSD score and accurate binding with target receptor. In this context, Crystal structure of glutathione s-transferase from *Escherichia coli* complexed with glutathionesulfonic acid ($C_{25}H_{38}O_4$) was tested with its co-crystallized glutathionesulfonic. RMSD = 0.001 Å.

DISCUSSION

The study of rhizospheric bacteria has revealed their potential as a source of bioactive metabolites bearing antimicrobial properties, particularly in the context of increasing antibiotic resistance.[27] In this investigation, rhizospheric bacteria were isolated and screened for antibacterial activity, agar overlay assay for

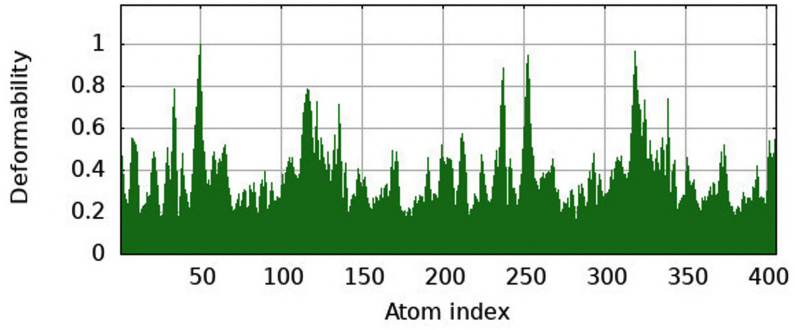
Deformability
1
0.8
0.6
0.4
0.2
0
50
100
150
200
250
300
350
400
Atom index

a

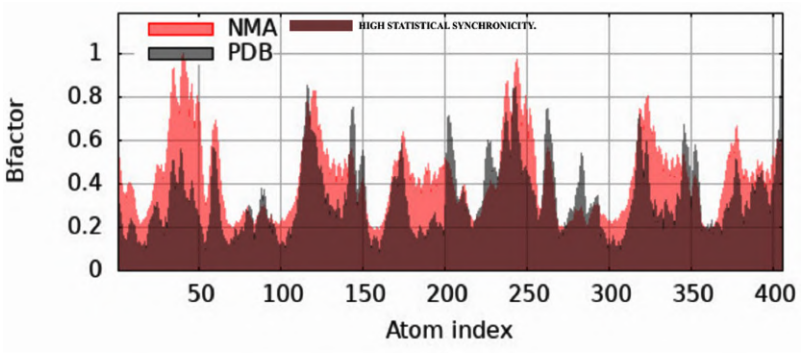
NMA
PDB
HIGH STATISTICAL SYNCHRONICITY.
Bfactor
1
0.8
0.6
0.4
0.2
0
50
100
150
200
250
300
350
400
Atom index

b

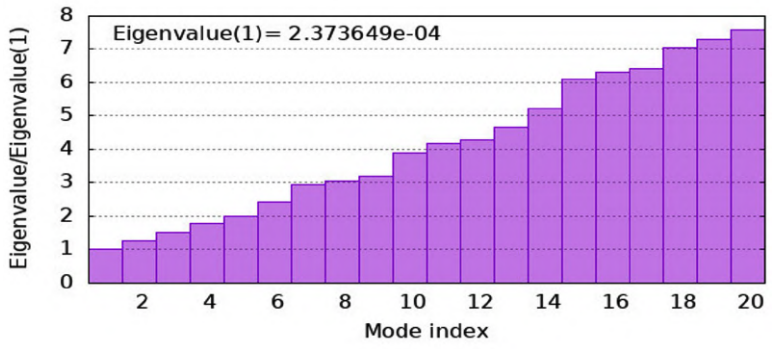
Eigenvalue(1)= 2.373649e-04
Eigenvalue/Eigenvalue(1)
8
7
6
5
4
3
2
1
0
2
4
6
8
10
12
14
16
18
20
Mode index

c

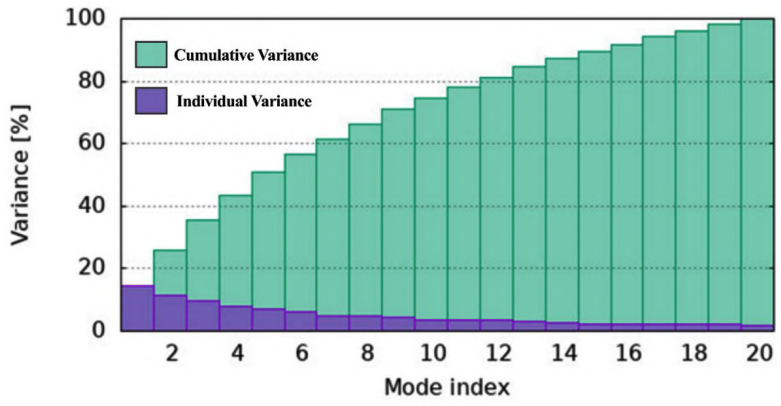
Cumulative Variance
Individual Variance
Variance [%]
100
80
60
40
20
0
2
4
6
8
10
12
14
16
18
20
Mode index

d

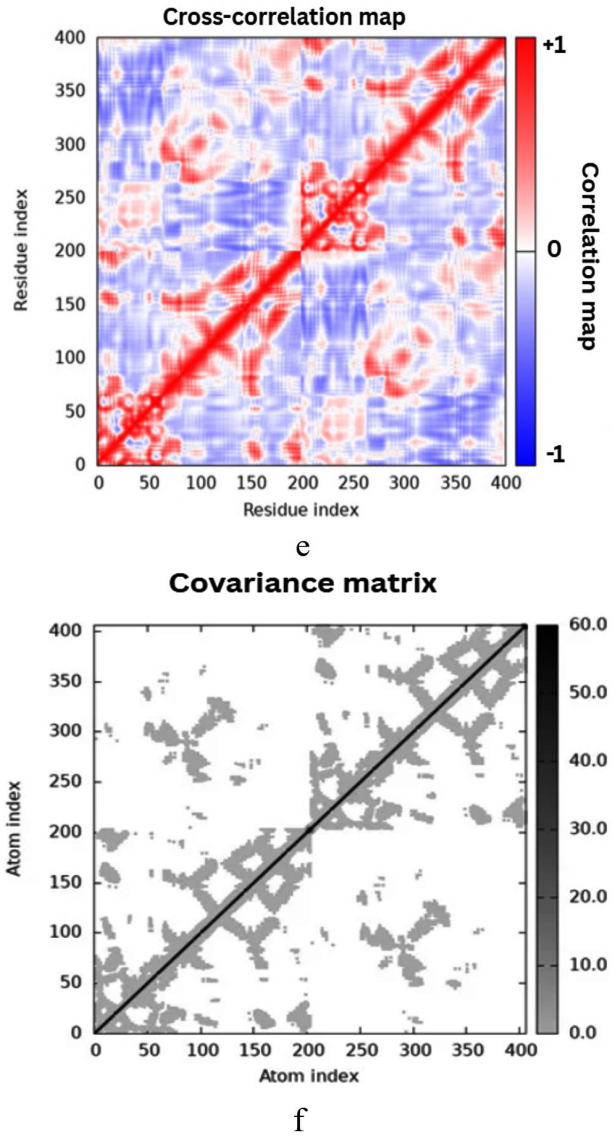

Figure 10. Molecular Dynamics Simulation Analysis of 1A0F (*E. coli* GST) (a) Deformability, (b) B-factor comparison, (c) Eigenvalues, (d) Variance, (e) Cross-correlation map, (f) Covariance matrix showing flexibility, motion correlations and atomic fluctuations

the screening of the rhizospheric bacteria in present study followed the protocol by Hockett and Baltrus.[28] Screening of bacteria *Burkholderia stagnalis* focusing on the antimicrobial property of secreated bioactive metabolites, in according to the previous research emphasising antimicrobial property of *Burkholderia paludis* sp. reported by Ong et al.[29] FTIR spectroscopy analysis of crude extract indicated peaks corresponding to various functional groups, including an N-H stretch at 3352 cm^{-1} (amine), Ca=N stretch at 2177 cm^{-1} (nitrile), and C=C stretches at 1637 cm^{-1} (aromatic/alkene), among others, which align with findings from previous work.[30] GC-MS analysis identified 24 bioactive metabolites from the bacterial crude extracts. Based on these data and comparison with the results of literature major bioactive metabolites were seen to bear antimicrobial property.[31]

The molecular docking studies conducted on bioactive metabolites derived from *Burkholderia stagnalis* revealed promising interactions with the GST protein of *E. coli*, a critical target in combating antimicrobial resistance (AMR). The docking score of the bioactive metabolite aligns with known *Burkholderia* metabolites like phenazine-1-carboxylic acid (produced by *Burkholderia stagnalis*-related strains), which exhibit antifungal/antibacterial activity, and pyrazine derivatives that disrupt microbial targets.[32] These findings are consistent with previous research that highlighted the antimicrobial efficacy of *Burkholderia* metabolites against various pathogens, including carbapenem-resistant strains, exhibit their potential in formulation of drug.[33,34] The evaluation of selected compounds for compliance with Lipinski's Rule of Five indicates their suitability for oral bioavailability, aligning with studies that emphasize the importance of pharmacokinetic properties in drug development. Toxicity assessments further classified the metab resolution in complex with a glutathione analogue metabolites based on administration routes, revealing that intravenous administration exhibited higher toxicity compared to oral routes, which is consistent with findings that suggest variations in toxicity profiles among different compounds.[35] Specifically, compounds like 1,3-Dioxolane and Cyclobutyl tridecyl phthalate demonstrated distinct LD_{50} values, reinforcing the need for thorough toxicity evaluations in the development of new antimicrobial agents. The applicability domain considerations further informed the reliability of toxicity predictions for these compounds by the method followed by Fisher et al.[36] The study highlighted Cyclobutyl tridecyl phthalate as a potent GST inhibitor. Rhizospheric bacteria, particularly *Burkholderia stagnalis*, are promising sources of natural bioactive metabolites as studied by Depoorter et al.[37] This aligns with previous findings that emphasize the role of *Burkholderia stagnalis* in producing bioactive metabolites effective against antibiotic-resistant pathogens.[38,39]

CONCLUSION

This study characterized antimicrobial metabolites from *Burkholderia stagnalis*, a rhizobacterium with genomic potential for diverse secondary metabolites. Computational docking identified cyclobutyl tridecyl phthalate as a high-affinity ligand (-8.9 kcal/mol) against *E. coli* glutathione S-transferase (GST), a virulence factor implicated in detoxification and antibiotic resistance. Partial purification validated bioactive fractions, consistent with genomic evidence of *Burkholderia*'s biosynthetic richness (>11% genome dedication in some species). The GST inhibition suggests a mechanism to potentiate existing antibiotics by countering resistance pathways, similar to cepacins or enacyloxins from related species. Further studies should integrate *in vitro* validation of GST inhibition with genome mining for novel clusters (e.g., NRPS, terpenes) and assess synergy with clinical drugs, leveraging *Burkholderia*'s documented capacity for antimicrobial biosynthesis.

ACKNOWLEDGMENTS

The authors thank the support from the Department of Biotechnology, Siddaganga Institute of Technology, Tumkur, under the grant National Network Project of Yenepoya (Deemed to be University), Mangalore. No. BT/PR40199/BTIS/137/89/2025 and for assistance in molecular docking and simulations.

CONFLICT OF INTEREST

The authors declare that there is no conflict of interest.

AUTHORS' CONTRIBUTION

All authors listed have made a substantial, direct and intellectual contribution to the work, and approved it for publication.

FUNDING

None.

DATA AVAILABILITY

The datasets generated and/or analysed during the current study are available from the corresponding author on reasonable request.

ETHICS STATEMENT

Not Applicable.

REFERENCES

1. Maithani D, Sharma A, Gangola S, Chaudhary P, Bhatt P. Insights into applications and strategies for discovery of microbial bioactive metabolites. *Microbiol Res*. 2022;261:127053. doi: 10.1016/j.micres.2022.127053
2. Gonzalez JM, Aranda B. Microbial Growth under Limiting Conditions-Future Perspectives. *Microorganisms*. 2023;11(7):1641 doi: 10.3390/microorganisms11071641
3. Bhattacharjya S, Ghosh A, Sahu A, et al. Utilizing soil metabolomics to investigate the untapped metabolic potential of soil microbial communities and their role in driving soil ecosystem processes: A review. *Appl Soil Ecol.* 2024;195:105238. doi: 10.1016/j.apsoil.2023.105238
4. Scoffone VC, Trespidi G, Barbieri G, Irudal S, Israyilova A, Buroni S. Methodological tools to study species of the genus *Burkholderia*. *Appl Microbiol Biotechnol.* 2021;105(24):9019-9034. doi: 10.1007/s00253-021-11667-3
5. Wallner A, King E, Ngonkeu ELM, Moulin L, Bena G. Genomic analyses of *Burkholderia cenocepacia* reveal multiple species with differential host-adaptation to plants and humans. *BMC Genomics.* 2019;20(1):803. doi: 10.1186/s12864-019-6186-z
6. Petrova YD, Mahenthiralingam E. Discovery, mode of action and secretion of *Burkholderia* sensu lato key antimicrobial specialised metabolites. *Cell Surf.* 2022;8:100081. doi: 10.1016/j.tcsw.2022.100081
7. Zakhour J, Ayoubi LWE, Kanj SS. Metallo-beta-lactamases: mechanisms, treatment challenges, and future prospects. *Expert Rev Anti Infect Ther.* 2024;22(4):189-201. doi: 10.1080/14787210.2024.2311213
8. Naghavi M, Vollset SE, Ikuta KS, et al. Global burden of bacterial antimicrobial resistance 1990–2021: a systematic analysis with forecasts to 2050. *Lancet*. 2024;404(10459):1199-1226. doi: 10.1016/s0140-6736(24)01867-1
9. Cedeno-Munoz JS, Aransiola SA, Reddy KV, et al. Antibiotic resistant bacteria and antibiotic resistance genes as contaminants of emerging concern: Occurrences, impacts, mitigations and future guidelines. *Science Total Environ.* 2024;952:175906. doi: 10.1016/j.scitotenv.2024.175906
10. Buldurun K, Aras A, Turan N, Turkan F, Adiguzel R, Bursal E. Synthesis and characterization of azo dye complexes as potential inhibitors of acetylcholinesterase, butyrylcholinesterase, and Glutathione S transferase. *ChemistrySelect*. 2022;7(40):e202203365. doi: 10.1002/slct.202203365
11. Balci N, Sakiroglu H, Turkan F, Bursal E. *In vitro* and *in silico* enzyme inhibition effects of some metal ions and compounds on glutathione S-transferase enzyme purified from *Vaccinium arctostapylous* L. *J Biomol Struct Dyn*. 2022;40(22):11587–11593. doi: 10.1080/07391102.2021.1960893
12. Wang F, Vasilyev V. *In silico* tuning of binding selectivity for new SARS-COV-2 main protease inhibitors. *Comput Methods Programs Biomed.* 2025;262:108678. doi: 10.1016/j.cmpb.2025.108678
13. Ibrahim SO, Ayipo YO, Lukman HY, et al. De novo in silico screening of natural products for antidiabetic drug discovery: ADMET profiling, molecular docking, and molecular dynamics simulations. *In Silico Pharmacol*. 2025;13(1):29. doi: 10.1007/s40203-025-00320-w
14. Kaliaperumal K, Salendra L, Liu Y, et al. Isolation of anticancer bioactive secondary metabolites from the sponge-derived endophytic fungi *Penicillium* sp. and *in-silico* computational docking approach. *Front Microbiol*. 2023;14:16928. doi: 10.3389/fmicb.2023.1216928
15. Nordstedt NP, Jones ML. Isolation of rhizosphere bacteria that improve quality and water stress tolerance in greenhouse ornamentals. *Front Plant Sci.* 2020;11:826. doi: 10.3389/fpls.2020.00826
16. Hossain TJ. Methods for screening and evaluation of antimicrobial activity: A review of protocols, advantages, and limitations. *Eur J Microbiol Immunol.* 2024;14(2):97-115. doi: 10.1556/1886.2024.00035
17. Damavandi MS, Shojaei H, Esfahani BN. The anticancer and antibacterial potential of bioactive secondary metabolites derived From bacterial endophytes in association with *Artemisia absinthium*. *Sci Rep*. 2023;13:18473. doi: 10.1038/s41598-023-45910-w
18. Megawati ER, Bangun H, Putra IB, et al. Phytochemical analysis by FTIR of *Zanthoxylum acanthopodium,* DC fruit ethanol extract, N-hexan, ethyl acetate and water fraction. *Med Arch.* 2023;77(3):183-188. doi: 10.5455/medarh.2023.77.183-188
19. Rakshith D, Santosh P, Pradeep TP et al. Application of Bioassay-Guided Fractionation Coupled with a Molecular Approach for the Dereplication of Antimicrobial Metabolites. *Chromatographia*. 2016;79:1625-1642. doi: 10.1007/s10337-016-3188-8
20. Syed B, Prasad MNN, Satish S. Synthesis and characterization of silver nanobactericides produced by *Aneurinibacillus migulanus* 141, a novel endophyte inhabiting Mimosa pudica L. *Arab J Chem.* 2016;12(8):3743-3752. doi: 10.1016/j.arabjc.2016.01.005
21. Azmal M, Paul JK, Prima FS, Talukder OF, Ghosh A. An *in silico* molecular docking and simulation study to identify potential anticancer phytochemicals targeting the RAS signaling pathway. *PLoS ONE.* 2024;19(9):e0310637. doi: 10.1371/journal.pone.0310637
22. Daina A, Michielin O, Zoete V. SwissADME: a free web tool to evaluate pharmacokinetics, drug-likeness and medicinal chemistry friendliness of small molecules. *Sci Rep*. 2017;7:42717. doi: 10.1038/srep42717
23. Duverna R, Ablordeppey SY, Lamango NS. Biochemical and Docking Analysis of Substrate Interactions with Polyisoprenylated Methylated Protein Methyl Esterase. *Curr Cancer Drug Targets.* 2010;10(6):634–648. doi: 10.2174/156800910791859443
24. Thai K-M, Le D-P, Tran N-V-K, Nguyen T-T-H, Tran T-D, Le M-T. Computational assay of Zanamivir binding affinity with original and mutant influenza neuraminidase 9 using molecular docking. *J Theor Biol.* 2015;385:31-39. doi: 10.1016/j.jtbi.2015.08.019
25. Thao TTP, Bui TQ, Quy PT, et al. Isolation, semi-synthesis, docking-based prediction, and bioassay-based activity of *Dolichandrone spathacea* iridoids: new catalpol derivatives as glucosidase inhibitors.

RSC Adv. 2021;11(20):11959-11975. doi: 10.1039/d1ra00441g

26. Lopez-Blanco JR, Aliaga JI, Quintana-Orti ES, Chacon P. iMODS: internal coordinates normal mode analysis server. *Nucleic Acids Res.* 2014;42:W271-W276. doi: 10.1093/nar/gku339
27. Pantigoso HA, Newberger D, Vivanco JM. The rhizosphere microbiome: Plant–microbial interactions for resource acquisition. *J Appl Microbiol.* 2022;133(5):2864-2876. doi: 10.1111/jam.15686
28. Hockett KL, Baltrus DA. Use of the soft-agar overlay technique to screen for bacterially produced inhibitory compounds. *J Vis Exp*. 2017;14(119):55064. doi: 10.3791/55064
29. Ong KS, Aw YK, Lee LH, Yule CM, Cheow YL, Lee SM. *Burkholderia paludis* sp. nov., an Antibiotic-Siderophore Producing Novel *Burkholderia cepacia* Complex Species, Isolated from Malaysian Tropical Peat Swamp Soil. *Front Microbiol*. 2016;7:02046. doi: 10.3389/fmicb.2016.02046
30. Verma R, Akanksha K, Jha SK, Rani L. Comparative studies of functional groups present in invasive and economically important plant leaf methanolic extracts by using FTIR spectroscopic analysis. *GSC Biol Pharm Sci*. 2023;23(03):184-191. doi: 10.5281/zenodo.8260419
31. Kim S, Chen J, Cheng T, et al. PubChem 2025 update. *Nucleic Acids Res*. 2024;53(D1):D1516-D1525. doi: 10.1093/nar/gkae1059
32. Rodríguez-Cisneros M, Morales-Ruíz LM, Salazar-Gómez A, Rojas-Rojas FU, Santos PEL. Compilation of the antimicrobial compounds produced by Burkholderia sensu stricto. *Molecules*, 2023;28(4):1646. doi: 10.3390/molecules28041646
33. Van Pelt C, Verduin CM, Goessens WHF, et al. Identification of *Burkholderia* spp. in the Clinical Microbiology Laboratory: Comparison of Conventional and Molecular Methods. *J Clin Microbiol.* 1999;37(7):2158-2164. doi: 10.1128/jcm.37.7.2158-2164.1999
34. Housh AB, Benoit M, Wilder SL, et al. Plant-Growth-Promoting Bacteria Can Impact Zinc Uptake in Zea mays: An Examination of the Mechanisms of Action Using Functional Mutants of *Azospirillum brasilense*. *Microorganisms*. 2021;9(5):1002. doi: 10.3390/microorganisms9051002
35. Li Y, Meng Q, Yang M, et al. Current trends in drug metabolism and pharmacokinetics. *Acta pharmaceutica Sinica. B.* 2019; 9(6):1113-1144. doi: 10.1016/j.apsb.2019.10.001
36. Fisher JL, Yamada K, Keebaugh AJ, et al. Evaluating Applicability Domain of Acute Toxicity QSAR models for military and industrial chemical risk assessment. *Toxicol Lett*. 2024;403:1-8. doi: 10.1016/j.toxlet.2024.11.006
37. Depoorter E, De Canck E, Coenye T, Vandamme P. *Burkholderia* Bacteria Produce Multiple Potentially Novel Molecules that Inhibit Carbapenem-Resistant Gram-Negative Bacterial Pathogens. *Antibiotics.* 2021;10(2):147. doi: 10.3390/antibiotics10020147
38. Selim MSM, Abdelhamid SA, Mohamed SS. Secondary metabolites and biodiversity of actinomycetes. *J Genet Eng Biotechnol.* 2021;19(1):72. doi: 10.1186/s43141-021-00156-9
39. Zhu X, Ning W, Xiao W, et al. Isolation and Identification of *Burkholderia stagnalis* YJ-2 from the Rhizosphere Soil of *Woodsia ilvensis* to Explore Its Potential as a Biocontrol Agent Against Plant Fungal Diseases. *Microorganisms.* 2025;13(6):1289. doi: 10.3390/microorganisms13061289